Title

Understanding Spatial Correlation Between Multiparametric MRI Performance and Prostate Cancer

Authors

Zabihollahy, Fatemeh
Naim, Sohaib
Wibulpolprasert, Pornphan
et al.

Publication Date

2024-02-12

DOI

10.1002/jmri.29287

Peer reviewed

Understanding Spatial Correlation Between Multiparametric MRI Performance and Prostate Cancer

Fatemeh Zabihollahy[1], PhD, Sohaib Naim[1,2], MS, Pornphan Wibulpolprasert[3], MD, Robert E. Reiter[4], MD, Steven S. Raman[1], MD, Kyunghyun Sung[1,2], PhD

[1] *Department of Radiological Sciences, David Geffen School of Medicine at UCLA, Los Angeles, CA, United States*
[2] *Physics, Biology in Medicine Interdisciplinary Program (IDP), David Geffen School of Medicine at UCLA, Los Angeles, CA, United States*
[3] *Department of Diagnostic and Therapeutic Radiology, Faculty of Medicine, Ramathibodi Hospital, 270 Rama VI Rd, Bangkok, Thailand 10400*
[4] *Department of Urology, David Geffen School of Medicine at UCLA, Los Angeles, CA, United States*

***Correspondence to:**

Fatemeh Zabihollahy, Ph.D.
Phone: (613) 890-6438
Zabihollahy.f@gmail.com

Grant Support: National Institutes of Health R01-CA248506 and R01-CA272702

Running Title: Spatial distribution of mpMRI performance for PCa diagnosis

ABSTRACT

Background: Multiparametric MRI (mpMRI) has shown a substantial impact on prostate cancer (PCa) diagnosis. However, the understanding of the spatial correlation between mpMRI performance and PCa location is still limited.

Purpose: To investigate the association between mpMRI performance and tumor spatial location within the prostate using a prostate sector map, described by Prostate Imaging Reporting and Data System (PI-RADS) v2.1.

Study type: Retrospective.

Subjects: 1,143 men who underwent mpMRI before radical prostatectomy between 2010 and 2022.

Field strength/sequence: 3.0 T. T2-weighted turbo spin-echo, a single-shot spin-echo EPI sequence for diffusion-weighted imaging, and a gradient echo sequence for dynamic contrast-enhanced MRI sequences.

Assessment: Integrated relative cancer prevalence (rCP), detection rate (DR), and positive predictive value (PPV) maps corresponding to the prostate sector map for PCa lesions were created. The relationship between tumor location and its detection/missing by radiologists on mpMRI compared to WMHP as a reference standard was investigated.

Statistical tests: A weighted chi-square test was performed to examine the statistical differences for rCP, DR, and PPV of the aggregated sectors within the zone, anterior/posterior, left/right prostate,

and different levels of the prostate with a statistically significant level of 0.05.

Results: A total of 1,665 PCa lesions were identified in 1,143 patients, and from those 1,060 lesions were clinically significant (cs)PCa tumors (any Gleason score (GS) ≥ 7). Our sector-based analysis utilizing weighted chi-square tests suggested that the left posterior part of PZ had a high likelihood of missing csPCa lesions at a DR of 67.0%. Aggregated sector analysis indicated that the anterior or apex locations in PZ had the significantly lowest csPCa detection at 67.3% and 71.5%, respectively.

Data conclusion: Spatial characteristics of the per-lesion-based mpMRI performance for diagnosis of PCa were studied. Our results demonstrated that there is a spatial correlation between mpMRI and locations of PCa on the prostate.

Keywords: Multiparametric MRI, Prostate cancer, Prostate sector map, PI-RADS, Whole-mount histopathology.

INTRODUCTION

Multiparametric magnetic resonance imaging (mpMRI) has been shown to be accurate for the diagnosis of prostate cancer (PCa) that requires treatment (1-3). Recent studies have shown the value of mpMRI prior to biopsy compared to random biopsies in men with elevated prostate-specific antigen (PSA) or abnormal digital rectal exam (DRE) for the increased detection rate (DR) of clinically significant PCa (csPCa) tumor (any Gleason score (GS) ≥ 7) while decreasing the diagnosis of csPCa (4-5), potentially obviating the need for biopsy (6-7). Thus, mpMRI before prostate biopsy in at-risk men is rapidly becoming the standard of care in clinical practice (8-9). However, it is crucial to investigate the accuracy and limitations of mpMRI for PCa detection.

Whole-mount histopathology (WMHP), which can be prepared after radical prostatectomy, is the ideal reference standard for correlating individual histopathologically confirmed PCa lesions to mpMRI findings to estimate mpMRI sensitivity for tumor detection. Johnson et al. compared the findings of mpMRI to WMHP as a reference standard to determine the pathologic characteristics of detected and missed PCa lesions by mpMRI (10). The results showed that the multifocality and size of PCa lesions are highly associated with the increased odds of missing tumors on mpMRI (10). A recent study by Wibulpolprasert et al. examined the spatial sensitivity of mpMRI for PCa localization and showed that mpMRI had significantly higher DR at the mid-gland or base than the apex (11-12). However, the spatial characteristics of PCa lesions associated with their detection/missing rate on mpMRI were not fully understood. For instance, it is not known if there is a difference between mpMRI performance for detecting tumors located in the posterior/anterior or left/right side of PZ vs.

TZ at different anatomical levels (10-12).

The purpose of this study is to 1) assess the spatial performance of mpMRI when detecting lesions with different pathologic characteristics, illustrated as relative cancer prevalence (rCP), DR, and positive predictive value (PPV) in a standardized prostate segmentation model, and 2) investigate whether there is any significant difference between mpMRI performance at different prostate locations for detecting PCa lesions with different pathology specifications. For the standardized prostate segmentation model, we used a sector map, described in Prostate Imaging Reporting and Data System (PI-RADS) v2.1, as a template to represent integrated rCP/DR/PPV maps (13).

MATERIALS AND METHODS

Study Population and MRI Analysis

This HIPAA-compliant study was approved by the local institutional review board (IRB) with a waiver of informed consent. Exclusion criteria were 1) patients with mpMRI performed at an outside facility, 2) prior prostate radiation, androgen deprivation therapy, or transurethral procedure, and 3) cases involving technical limitations. A total of 1,143 consecutive patients who underwent 3T mpMRI before robotic-assisted radical prostatectomy (RALP) were included at a single institution between 2010 and 2022.

All patients underwent prostate MRI, according to a standardized protocol, including T2-weighted turbo spin-echo (T2-TSE), a single-shot spin-echo EPI sequence for diffusion-weighted imaging (DWI), and a gradient echo sequence for dynamic contrast-enhanced (DCE) MRI sequences, on one of the following MRI scanners (Magnetom Trio, Skyra, or Verio, all from Siemens Healthineers, Erlangen, Germany). As part of the standard of care,

each mpMRI study was interpreted by abdominal imaging fellows confirmed by board-certified genitourinary (GU) abdominal imaging subspecialized radiologists. The radiologists performed assessments using a 5-point scale based on PI-RADS, in which a category 1 lesion indicated a very low suspicion for clinically significant PCa, whereas a category 5 lesion was very highly suspicious for clinically significant PCa.

All suspicious lesions were contoured within the prostate on T2W MRI as a main sequence (by S.S.R. with 26 years of experience) and mapped on DWI and DCE via cognitive registration (by P.W. with 10 years of experience). The PCa contours were then manually mapped to the 41-segmentation PI-RADS prostate sector map [13].

Histopathology Analysis

Thin-section WMHP was prepared by experienced GU pathology technicians, by slicing each prostate gland from the apex to the base in 5-mm increments in the axial plane. Each slice was photographed on both the basal and apical sides and fixed for another 24 hours and then underwent whole-mount paraffin embedding and interpreted by a dedicated experienced GU pathologist independently of preoperative MRI findings before subsequent correlation. The genitourinary pathologist delineated all PCa lesions, including the largest diameter, location, primary and secondary GS, and relationship to the capsule, veins, and nerves. The guidelines issued by the International Society of Urological Pathology (ISUP) were used for the grading of prostate cancer (14), and clinically significant PCa (csPCa) was defined as a lesion with an ISUP grade 2 or higher (15). The index lesion was defined as the PCa lesion with the highest ISUP grade or the largest size or both. PCa lesions with a diameter of $\geq$ 1.5 cm were considered large tumors.

Radiology-pathology Correlation

GU radiologists and pathologists re-reviewed each previously detected and graded lesion on mpMRI and WMHP and collectively determined concordance in the monthly radiologic-pathologic match meetings. Figure 1 illustrates the radiology-pathology matching workflow with mpMRI and WMHP using the prostate sector map for one patient. For each lesion, mpMRI was compared to the corresponding WMHP slide. A lesion that appeared on both mpMRI and WMHP was labeled as true positive (TP), and its sectors were recorded based on the appearance on mpMRI (1: TP in Fig 1). A lesion that was shown on mpMRI but not on WMHP was categorized as false positive (FP), and its sectors were recorded based on the appearance on mpMRI (2: FP in Fig 1). Lastly, a lesion that was shown only on WMHP was classified as false negative (FN), and its sectors were assigned based on their appearance on WMHP (3: FN in Fig 1). This process has been repeated for all lesions in 1143 patients. Labeled lesions (TP, FN, and FP) were compared to the prostate sector map to extract spatial information for each tumor.

Collecting all information yielded the total number and weighted sum of TP, FP, and FN lesions in each segment of the sector map, which was used to obtain the per-lesion and per-sector-based diagnostic performance of mpMRI. To calculate rCP, the number of lesions in each region of the sector map was divided by the total number of PCa lesions (TP+FN) stratified by pathologic characterization. DR and PPV were computed as TP/(TP+FN) and TP/(TP+FP), respectively. rCP, DR, and PPV values were sorted from all sectors, and the distributions of high rCP and low DR and PPV values were identified in the integrated rCP/DR/PPV maps.

Statistical Analysis

The spatial distribution of the PCa tumors on the prostate whole gland was investigated to determine whether there is a major difference in the zone, anterior/posterior direction, and levels of the prostate. To this end, radiology-pathology correlation was performed to measure DR and PPV across different sectors with different pathology characteristics (ISUP ≥ 1, 2, and 3, index, large PCa, etc.). A weighted chi-square test was performed to examine the statistical differences for rCP, DR, and PPV of the aggregated sectors within the zone (TZ/PZ), anterior/posterior, left/right prostate, and different levels of the prostate (base, mid, and apex). All data was analyzed via SPSS v23 (IBM SPSS Statistics, Armonk, NY), to calculate the metrics and perform statistical analysis with a statistically significant level of 0.05.

RESULTS

The final study cohort included 1,143 patients (age = 61.96±7.03 years, weight = 86.44±13.74 kg, PSA = 7.71±7.47 ng/mL, and prostate volume = 41.70±19.20 cm^3; mean ± standard deviation). A total of 1,665 PCa lesions (TP and FN) at WMHP were identified, where the average number of PCa lesions per patient was 1.5 (Tables 1-4). Of 1,665 PCa lesions, 64% and 25% (1,060 and 414) were ISUP grade ≥ 2 and ≥ 3. Overall, the majority of cancer lesions were located on the PZ with an approximate ratio of 3:1, consistent across different ISUP grades. Investigating the relative distribution of cancer lesions in the anterior and posterior parts of the prostate revealed that the proportion of cancer lesions in the posterior part increased by the ISUP grades (62%, 66%, and 70% for tumors with ISUP grade ≥ 1, 2, and 3, respectively). The prostate cancer distribution at different levels of the prostate (base,

mid, and apex) was approximately 15%, 50%, and 35%, respectively, and did not change much by the ISUP grades.

The sector-based spatial characteristics of mpMRI are shown for the diagnosis of csPCa (Figure 2) and index csPCa (Figure 3) lesions. The per-sector-based rCP, DR, and PPV values are shown, and the sectors belonging to the 75th percentile and higher of rCP and the 25th percentile and lower of DR and PPV are represented in red. The performance of mpMRI for diagnosis of csPCa and index csPCa varied across sectors, but a similar spatial pattern of high relative cancer occurrences was observed in posterior PZ at the mid-gland and apex prostate levels (539/1,060 or 51% for csPCa lesions; 430/846 or 51% for index csPCa lesions) and low relative cancer occurrences in posterior TZ at every prostate level (53/1,060 or 5% for csPCa lesions; 46/846 or 5% for index csPCa lesions). The left posterior part of PZ was part of the lowest DR group with a DR of 67% for csPCa and 70% for index csPCa (both within 0^{th}-25^{th} percentiles) while within the highest cancer occurrence group at 5% for csPCa and 5% for index csPCa (both within 75^{th} -100^{th} percentiles), suggesting the likelihood of missing cancer lesions here is high. Interestingly, the same area, left posterior PZ, was also part of the lowest PPV group of the index csPCa lesions at 69% (0^{th} -25^{th} percentile), indicating potential overdiagnosis at the same time.

Cancer detection increased with ISUP grades (63%, 73%, and 78% for tumors with ISUP grade $\geq$ 1, 2, and 3, respectively). No significant difference in DRs was observed between TZ and PZ for any ISUP grade group (p=0.27 at ISUP grade $\geq$ 1; p=0.39 at ISUP grade $\geq$ 2; p=0.87 at ISUP grade $\geq$ 2 and index; p=0.193 at ISUP grade $\geq$ 3). Significant differences were observed between anterior vs. posterior, and levels of the prostate, separately within TZ

and PZ in detecting PCa, which stayed similar only in PZ, for detecting csPCa and index csPCa. In PZ, the lowest DR was 67% for csPCa lesions in the anterior location, significantly different from the posterior location of 76%. For different levels of the prostate, csPCa lesions at the apex had the lowest DR at 71%.

The PPVs decreased with ISUP grades (91%, 81%, and 37% for tumors with ISUP grade ≥ 1, 2, and 3, respectively). A significant difference was noticed in PPV between TZ and PZ, regardless of ISUP grades or index lesions. In PZ, lesions at the base had the lowest PPVs, showing the difference across different levels of the prostate (87% at ISUP grade ≥ 1; 77% at ISUP grade ≥ 2; 70% at ISUP grade ≥ 2 and index). For ISUP grade ≥ 3, PPVs for anterior/posterior lesions were significantly different in TZ. For large-sized lesions, sector-based spatial characteristics are illustrated in Supplementary Tables 1 and 2.

DISCUSSION

We studied the spatial characteristics of PCa lesions associated with mpMRI detection in correlation with WMHP using the largest dataset to date. The prostate sector map described by PI-RADS v2-1 was used as a standardized prostate segmentation template to visualize mpMRI performance in terms of rCP, DR, and PPV for lesions with pathology specifications. Overall, mpMRI detected 63% of tumors with ISUP ≥ 1. The DR of mpMRI significantly improved for intermediate and severe tumors with ISUP ≥ 2, and 3 (DR of 73% and 78%, respectively), while PPV of 91% decreased with ISUP grades (81% and 37% for ISUP ≥ 2 and ISUP ≥ 3, respectively).

Conventionally, a random systematic biopsy of the entire prostate gland is performed for men

with high PSA or abnormal DRE, wherein many samples of tissue are randomly sampled from different areas of the prostate. The main disadvantage of random biopsy is that it results in up to 30% false negative (when a tumor was not sampled) (16-18) and may underestimate the aggressiveness of cancer through insufficient sampling (19-22). Our results may reduce the need for random systematic prostate biopsy as it indicates areas with the highest rCP, where samples can be removed, which in turn may improve PCa diagnosis by reducing the false-negative rates.

The outcomes of this study characterize disease appearance relative to the prostate zones and lobes (i.e., anterior, and posterior). Compared to the prostate cancer atlas that integrates information on PCa tumors across multiple patients into a single canonical representation, the rCP map illustrates mpMRI performance stratified by tumor pathology specifications. Additionally, the results provide DR and PPV information for each segment of the prostate sector map, which is missing information on the PCa atlas. This distinction is important because sector-based DR/PPV metrics facilitate the realization of mpMRI limitations for tumor detection classified by tumor aggressiveness and reveal regions of the prostate where most erroneous diagnoses happen.

In recent years, computer-aided diagnosis (CAD) tools developed for automated diagnosis of PCa using mpMRI (REF). Defining high rCP and low DR regions can be considered as prior information for CAD tools. Incorporating the findings of this study (i.e., high rCP and low DR regions) may lead to more accurate and precise performance of CAD tools, as prior information will reduce the generalization errors of artificial intelligence (AI) (23). Merging this information with the AI-based methods designed for automated localization of PCa lesions particularly increases the sensitivity via directing attention to the predominant regions

in mpMRI for PCa existence.

Our study showed that the anterior or apex locations in PZ had the lowest csPCa detection while a base location in PZ had the lowest PPV, revealing mpMRI limitations in under- and over-detection of PCa. The potential reason can be compromised image contrast due to partial volume between a prostate lesion and surrounding tissue at the base and apex anatomical levels, resulting in reduced cancer invisibilities at those levels.

Limitations

First, the study cohort was within a surgical population as WMHP was required for comparison, which may create the potential to include selection biases in population and/or cancer prevalence. Second, using PPV with a high prevalence of PCa, as PPV is not just intrinsic to the test but also depends on the disease prevalence. To avoid interpreting high PPV as an indicator of high accuracy for such statistics, PPV was reported along with the detection rate and relative cancer prevalence rate. Third, although an rCP map has been created for PCa lesions with different pathology specifications, the information is provided only at the base, mid-gland, and apex levels, which can be considered as a low-resolution/2-D basis prostate cancer atlas. Integrating the results of this study with a 3-D prostate cancer atlas along with an MR-based registration framework will address this issue and supply improved information for clinicians, which is the next step of our current study. Fourth, our results are from a high-volume academic institution with substantial expertise in image acquisition and prostate mpMRI interpretation, which might render an optimistic result for PCa detection using mpMRI compared to lower-volume, less-experienced community centers. Fifth, only WMHP was used as a reference standard to find the location of the PCa tumor on the prostate.

However, including the results of the biopsy might be beneficial as some small lesions may be almost removed during the biopsy, which is difficult to evaluate in the whole prostate specimen after radical prostatectomy.

Conclusion

Our study demonstrated that there is a spatial correlation between mpMRI performance and the location of PCa tumors on the prostate, indicating that the anterior or apex/base locations in PZ had the lowest cancer detection while a base location in PZ had the lowest PPV. These findings can potentially provide a visual guideline for improved PCa diagnosis by drawing clinicians' attention to these identified locations.

ACKNOWLEDGEMENT

This research was funded in part by the National Institutes of Health under grants R01-CA248506 and R01-CA272702 and by the Integrated Diagnostics Program of the Departments of Radiological Sciences and Pathology in the UCLA David Geffen School of Medicine.

REFERENCES

1. Futterer JJ, Briganti A, De Visschere P, et al. Can Clinically Significant Prostate Cancer Be Detected with Multiparametric Magnetic Resonance Imaging? A Systematic Review of the Literature. Eur Urol 2015;68:1045–1053.
2. Chamie K, Sonn GA, Finley DS, et al. The role of magnetic resonance imaging in delineating clinically significant prostate cancer. Urol 2014;83:369–375.
3. Lee DH, Koo KC, Lee SH, et al. Low-risk prostate cancer patients without visible tumor (T1c) on multiparametric MRI could qualify for active surveillance candidate even if they did not meet inclusion criteria of active surveillance protocol. Jpn J Clin Oncol 2013;43:553–558.
4. Ahmed HU, El-Shater Bosaily A, Brown LC, et al. Diagnostic accuracy of multi-parametric MRI and TRUS biopsy in prostate cancer (PROMIS): a paired validating confirmatory study. Lancet 2017;389:815–822.
5. Kasivisvanathan V, Rannikko AS, Borghi M, et al. MRI-targeted or standard biopsy for prostate-cancer diagnosis. N Engl J Med 2018; 378:1767-1777.
6. Mehralivand S, Shih JH, Rais-Bahrami S, et al. A magnetic resonance imaging-based prediction model for prostate biopsy risk stratification. JAMA Oncol 2018;4:678–85.
7. Moldovan PC, Van den Broeck T, Sylvester R, et al. What is the negative predictive value of multiparametric magnetic resonance imaging in excluding prostate cancer at biopsy? A systematic review and meta-analysis from the European Association of Urology prostate cancer guidelines panel. Eur Urol 2017;72:250–66.
8. Washino S, Kobayashi S, Okochi T, et al. Cancer detection rate of prebiopsy MRI

with subsequent systematic and targeted biopsy are superior to non-targeting systematic biopsy without MRI in biopsy naïve patients: a retrospective cohort study. BMC Urol 2018;18:51.

9. Faria R, Soares MO, Spackman E, et al. Optimising the diagnosis of prostate cancer in the era of multiparametric magnetic resonance imaging: a cost-effectiveness analysis based on the prostate MR imaging study (PROMIS). Eur Urol 2018;73:23–30.
10. Johnson DC, Raman SS, Mirak SA, et al. Detection of Individual Prostate Cancer Foci via Multiparametric Magnetic Resonance Imaging. Eur Urol 2019;75:712–720.
11. Wibulpolprasert P, Raman SS, Hsu W, et al. Detection and Localization of Prostate Cancer at 3-T Multiparametric MRI Using PI-RADS Segmentation. AJR 2019; 212: W122-W131.
12. Wibulpolprasert P, Raman SS, Hsu W, et al. Influence of the Location and Zone of Tumor in Prostate Cancer Detection and Localization on 3-T Multiparametric MRI Based on PI-RADS Version 2. AJR 2020;214:1101-1111.
13. American College of Radiology. PI-RADSTM Prostate Imaging- Reporting and Data System. ACR; 2019 https://www.acr.org/-/media/ACR/Files/RADS/Pi-RADS/PIRADS-V2-1.pdf.
14. Egevad L, Delahunt B, Srigley JR 4, Samaratunga H. International Society of Urological Pathology (ISUP) grading of prostate cancer - An ISUP consensus on contemporary grading. APMIS. 2016;124:433-5.
15. Seo JW, Shin SJ, Taik Oh Y, et al. PI-RADS Version 2: Detection of Clinically Significant Cancer in Patients with Biopsy Gleason Score 6 Prostate Cancer. AJR Am J Roentgenol

2017;209:W1-W9.

16. Serefoglu EC, Altinova S, Ugras NS, Akincioglu E, Asil E, Balbay MD. How reliable is 12-core prostate biopsy procedure in the detection of prostate cancer? J Can Urol Assoc. 2013;7:E293–E298.
17. Rabbani F, Stroumbakis N, Kava BR, Cookson MS, Fair WR. Incidence and clinical significance of false-negative sextant prostate biopsies. J Urol. 1998;159:1247–1250.
18. Bjurlin MA, Carter HB, Schellhammer P, et al. Optimization of initial prostate biopsy in clinical practice: sampling, labeling and specimen processing. J Urol. 2013;189:2039–2046.
19. Presti JC. Prostate biopsy: current status and limitations. Rev Urol 2007;9:93–98.
20. Corcoran NM, Hovens CM, Hong MKH, et al. Underestimation of Gleason score at prostate biopsy reflects sampling error in lower volume tumors. BJU Int 2012;109:660–664.
21. Moreira Leite KR, Camara-Lopes LHA, Dall'Oglio MF, et al. Upgrading the Gleason score in extended prostate biopsy: implications for treatment choice. Int J Radiat Oncol Biol Phys 2009;73:353–356.
22. Sadoughi N, Krishna S, McInnes MDF, et al. ADC metrics from multiparametric MRI: histologic downgrading of Gleason score 9 or 10 prostate cancers diagnosed at nontargeted transrectal ultrasound-guided biopsy. AJR Am J Roentgenol 2018;211:W158–W165.
23. Gulcehre C, Bengio Y. Knowledge Matters: Importance of Prior Information for Optimization. Journal of Machine Learning Research 2016;17:1-32.

TABLES

Table 1. Performance of mpMRI for detecting prostate cancer (PCa) lesions with ISUP grade ≥ 1.

PI-RADS ≥ 3 & ISUP grade ≥ 1	Number of Cancer Lesions (TP/FN)			1665 (873/792)	
	Number of FP Lesions			209	
	Prostate Cancer Distribution			Value	
	Relative Cancer Prevalence (%)	Transition Zone (TZ)		22.8	
		Peripheral Zone (PZ)		71.0	
		Anterior		38.2	
		Posterior		61.5	
		Base		14.4	
		Mid		49.7	
		Apex		35.6	
	Diagnostic Performance of mpMRI			Value	p-value
	Detection Rate (%)	Whole Prostate		63.0	-
		Transition Zone		62.0	0.27
		Peripheral Zone		63.7	
		TZ	Anterior	58.7	<0.001*
			Posterior	70.6	
			Left	65.4	0.010*
			Right	58.7	
			Base	72.2	<0.001*
			Mid	61.7	
			Apex	54.6	
		PZ	Anterior	51.3	<0.001*
			Posterior	67.3	
			Left	62.6	0.161
			Right	64.7	
			Base	64.3	<0.001*
			Mid	66.1	
			Apex	60.2	
	Positive Predictive Value (%)	Whole Prostate		90.6	-
		Transition Zone		88.3	0.007*
		Peripheral Zone		91.2	
		TZ	Anterior	89.3	0.162
			Posterior	86.3	
			Left	87.1	0.180
			Right	89.8	
			Base	90.2	0.73
			Mid	88.1	
			Apex	89.2	
		PZ	Anterior	94.6	0.002*
			Posterior	90.5	
			Left	90.5	0.154
			Right	91.9	
			Base	87.1	<0.001*
			Mid	90.9	
			Apex	93.1	

** TP: true positive; FN: false negative; FP: false positive.

Table 2. Performance of mpMRI for detecting clinically significant prostate cancer (csPCa) lesions.

PI-RADS ≥ 3 & ISUP grade ≥ 2	Number of Cancer Lesions (TP/FN)			1060 (749/311)	
	Number of FP Lesions			333	
	Prostate Cancer Distribution			Value	
	Relative Cancer Prevalence (%)	Transition Zone (TZ)		21.5	
		Peripheral Zone (PZ)		72.1	
		Anterior		34.2	
		Posterior		65.4	
		Base		14.8	
		Mid		50.5	
		Apex		34.3	
	Diagnostic Performance of mpMRI			Value	p-value
	Detection Rate (%)	Whole Prostate		73.4	-
		Transition Zone		72.6	0.39
		Peripheral Zone		74.0	
		TZ	Anterior	71.6	0.33
			Posterior	74.6	
			Left	75.7	0.025*
			Right	69.4	
			Base	74.4	0.30
			Mid	73.5	
			Apex	69.5	
		PZ	Anterior	67.3	<0.001*
			Posterior	75.6	
			Left	73.3	0.39
			Right	74.6	
			Base	73.2	0.003*
			Mid	75.9	
			Apex	71.5	
	Positive Predictive Value (%)	Whole Prostate		81.1	-
		Transition Zone		75.8	<0.001*
		Peripheral Zone		82.4	
		TZ	Anterior	75.1	0.49
			Posterior	77.1	
			Left	74.4	0.28
			Right	77.4	
			Base	71.7	0.42
			Mid	76.6	
			Apex	76.2	
		PZ	Anterior	85.0	0.086
			Posterior	81.9	
			Left	81.8	0.40
			Right	83.0	
			Base	77.1	0.005*
			Mid	82.5	
			Apex	84.1	

** TP: true positive; FN: false negative; FP: false positive.

Table 3. Performance of mpMRI for detecting index clinically significant prostate cancer (csPCa) lesions.

PI-RADS ≥ 3 & ISUP grade ≥ 2 & Index	Number of Cancer Lesions (TP/FN)			846 (653/193)	
	Number of FP Lesions			429	
	Prostate Cancer Distribution			Value	
	Relative Cancer Prevalence (%)	Transition Zone (TZ)		21.5	
		Peripheral Zone (PZ)		71.6	
		Anterior		33.5	
		Posterior		66.0	
		Base		15.8	
		Mid		49.4	
		Apex		34.3	
	Diagnostic Performance of mpMRI			Value	p-value
	Detection Rate (%)	Whole Prostate		76.5	-
		Transition Zone		76.9	0.87
		Peripheral Zone		76.6	
		TZ	Anterior	78.1	0.26
			Posterior	74.8	
			Left	79.0	0.106
			Right	74.5	
			Base	73.8	0.128
			Mid	80.2	
			Apex	75.2	
		PZ	Anterior	72.7	0.015*
			Posterior	77.5	
			Left	75.9	0.38
			Right	77.3	
			Base	71.6	<0.001*
			Mid	79.4	
			Apex	74.4	
	Positive Predictive Value (%)	Whole Prostate		75.1	-
		Transition Zone		70.9	0.003*
		Peripheral Zone		75.7	
		TZ	Anterior	69.3	0.143
			Posterior	73.8	
			Left	70.3	0.69
			Right	71.5	
			Base	69.4	0.88
			Mid	70.4	
			Apex	71.5	
		PZ	Anterior	78.9	0.059
			Posterior	75.0	
			Left	74.8	0.26
			Right	76.5	
			Base	69.5	0.002*
			Mid	75.6	
			Apex	77.9	

** TP: true positive; FN: false negative; FP: false positive.

Table 4. Performance of mpMRI for detecting prostate cancer (PCa) lesions with ISUP grade ≥ 3.

PI-RADS ≥ 3 & ISUP grade ≥ 3	Number of Cancer Lesions (TP/FN)			414 (331/83)	
	Number of FP Lesions			751	
	Prostate Cancer Distribution			Value	
	Relative Cancer Prevalence (%)	Transition Zone (TZ)		20.6	
		Peripheral Zone (PZ)		73.3	
		Anterior		29.4	
		Posterior		69.7	
		Base		15.3	
		Mid		49.4	
		Apex		34.5	
	Diagnostic Performance of mpMRI			Value	p-value
	Detection Rate (%)	Whole Prostate		78.4	-
		Transition Zone		76.3	0.193
		Peripheral Zone		79.3	
		TZ	Anterior	77.5	0.48
			Posterior	74.6	
			Left	80.6	0.034*
			Right	71.8	
			Base	76.5	0.92
			Mid	75.6	
			Apex	77.3	
		PZ	Anterior	77.0	0.34
			Posterior	79.7	
			Left	81.1	0.074
			Right	77.3	
			Base	80.8	0.83
			Mid	79.1	
			Apex	78.8	
	Positive Predictive Value (%)	Whole Prostate		37.4	-
		Transition Zone		32.2	<0.001*
		Peripheral Zone		39.0	
		TZ	Anterior	28.0	<0.001*
			Posterior	40.2	
			Left	31.6	0.66
			Right	32.9	
			Base	25.6	0.006*
			Mid	28.6	
			Apex	36.7	
		PZ	Anterior	39.3	0.89
			Posterior	39.0	
			Left	41.1	0.020*
			Right	37.0	
			Base	37.7	0.179
			Mid	38.2	
			Apex	40.8	

** TP: true positive; FN: false negative; FP: false positive.

Figure Legends

Figure 1: Workflow of our spatial correlation method, including the identification of TP/FN/FP lesions by matching radiology and pathology findings and the creation of integrated rCP/DR/PPV maps using the standardized segmentation sector map.

Figure 2. From left to right, relative cancer prevalence, detection rate, and positive predictive value heatmaps of csPCa lesions at the basal, mid, and apex levels, corresponding to the prostate sector map. The red color shows the 75th percentile or higher values of rCP and the 25^{th} percentile of lower values of DR and PPV value on the sector map, respectively.

Figure 3. From left to right, relative cancer prevalence, detection rate, and positive predictive value heatmaps of index csPCa lesions at the basal, mid, and apex levels, correspond to the prostate sector map. The red color shows the 75th percentile or higher values of rCP and the 25^{th} percentile of lower values of DR and PPV value on the sector map, respectively.

FIGURE CAPTIONS

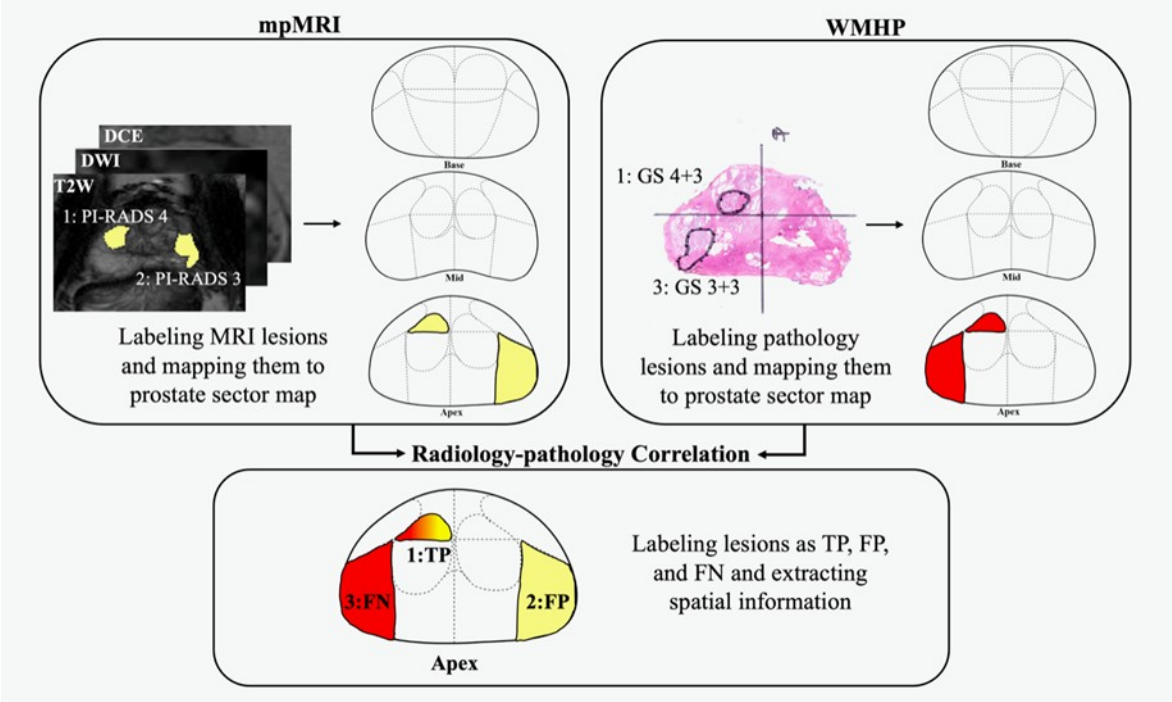

Figure 1: Workflow of our spatial correlation method, including the identification of TP/FN/FP lesions by matching radiology and pathology findings and the creation of integrated rCP/DR/PPV maps using the standardized segmentation sector map.

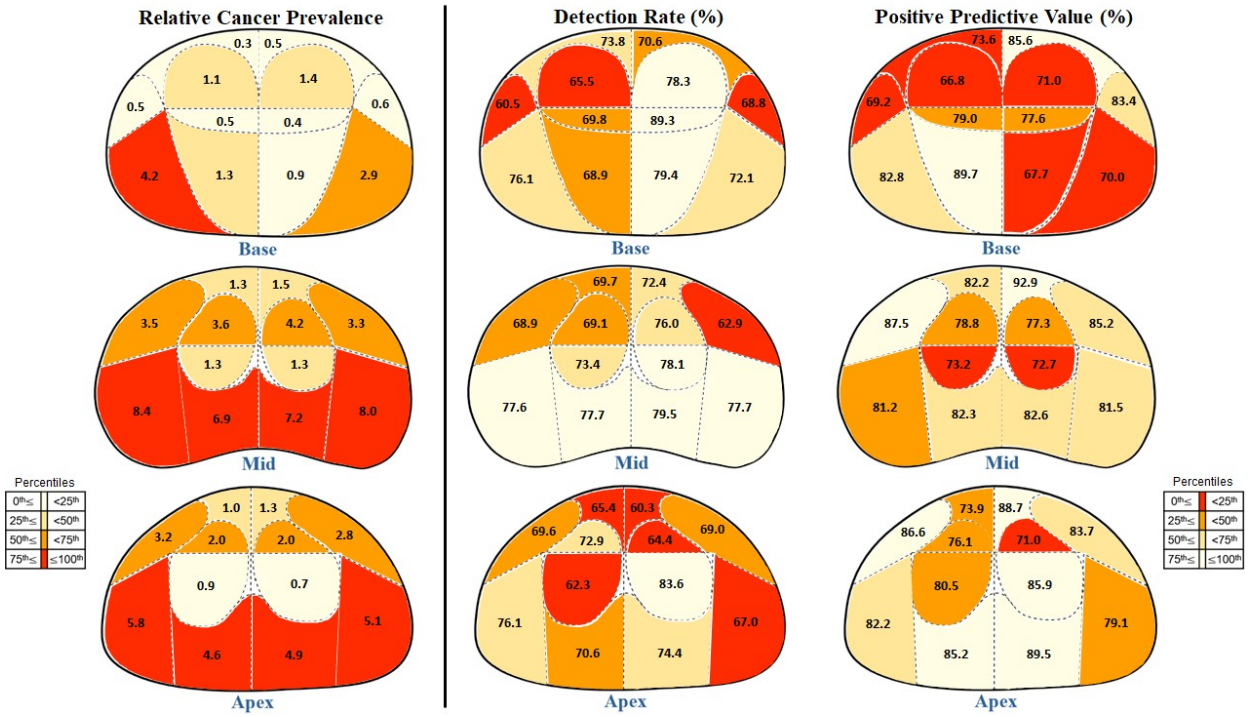

Figure 2. From left to right, relative cancer prevalence, detection rate, and positive predictive value heatmaps of csPCa lesions at the basal, mid, and apex levels, correspond to the prostate sector map. The red color shows the 75th percentile or higher values of rCP and the 25th percentile of lower values of DR and PPV value on the sector map, respectively.

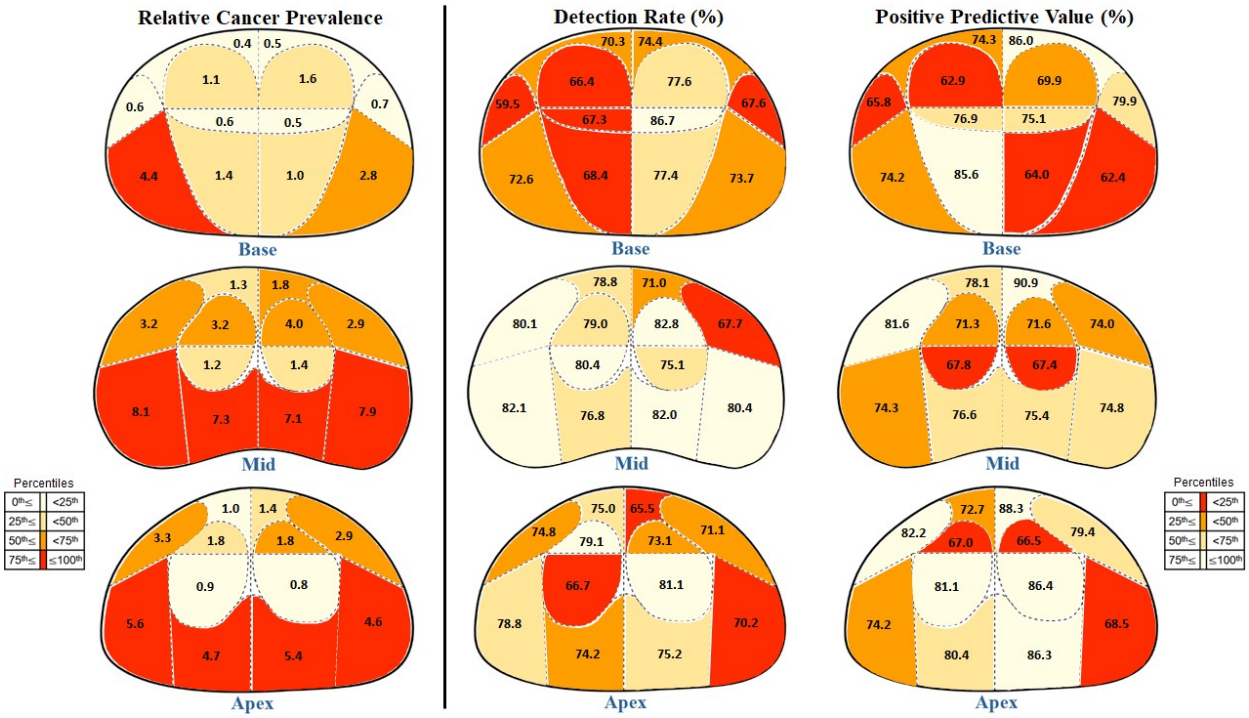

Figure 3. From left to right, relative cancer prevalence, detection rate, and positive predictive value heatmaps of index csPCa lesions at the basal, mid, and apex levels, correspond to the prostate sector map. The red color shows the 75th percentile or higher values of rCP and the 25th percentile of lower values of DR and PPV value on the sector map, respectively.

Supplementary Table 1. Performance of mpMRI for detecting large csPCa lesions (tumor diameter ≥ 1.5 cm).

PI-RADS ≥ 3 & ISUP grade ≥ 2 & Large	Number of Cancer Lesions (TP/FN)			725 (579/146)	
	Number of FP Lesions			503	
	Prostate Cancer Distribution			Value	
	Relative Cancer Prevalence (%)	Transition Zone		23.6	
		Peripheral Zone		69.4	
		Anterior		36.0	
		Posterior		63.4	
		Base		15.7	
		Mid		50.4	
		Apex		33.4	
	Diagnostic Performance of mpMRI			Value	p-value
	Detection Rate (%)	Whole Prostate		77.5	-
		Transition Zone		77.5	1.00
		Peripheral Zone		77.5	
		TZ	Anterior	78.8	0.181
			Posterior	74.9	
			Left	81.6	0.002*
			Right	73.0	
			Base	76.7	0.160
			Mid	79.8	
			Apex	74.3	
		PZ	Anterior	74.2	0.041*
			Posterior	78.3	
			Left	77.4	0.93
			Right	77.5	
			Base	79.4	<0.001*
			Mid	80.3	
			Apex	72.8	
	PPV (%)	Whole Prostate		70.4	-
		Transition Zone		70.2	0.67
		Peripheral Zone		69.5	
		TZ	Anterior	70.3	0.97
			Posterior	70.1	
			Left	70.3	0.97
			Right	70.2	
			Base	70.3	1.00
			Mid	70.6	
			Apex	70.4	
		PZ	Anterior	76.5	<0.001*
			Posterior	68.0	
			Left	68.8	0.43
			Right	70.1	
			Base	67.3	0.47
			Mid	70.3	
			Apex	69.1	

Supplementary Table 2. Performance of mpMRI for detecting large index csPCa lesions (tumor diameter ≥ 1.5 cm).

PI-RADS ≥ 3 & ISUP grade ≥ 2 & Large & Index	Number of Cancer Lesions (TP/FN)			664 (537/127)	
	Number of FP Lesions			545	
	Prostate Cancer Distribution			Value	
	Relative Cancer Prevalence (%)	Transition Zone		23.2	
		Peripheral Zone		69.2	
		Anterior Lateral		35.4	
		Posterior Lateral		63.9	
		Base		16.0	
		Mid		49.7	
		Apex		33.6	
	Diagnostic Performance of mpMRI			Value	p-value
	Detection Rate (%)	Whole Prostate		78.3	-
		Transition Zone		79.0	0.60
		Peripheral Zone		78.2	
		TZ	Anterior	81.3	0.033*
			Posterior	75.1	
			Left	82.0	0.027*
			Right	75.8	
			Base	77.5	0.043*
			Mid	82.5	
			Apex	75.5	
		PZ	Anterior	75.6	<0.001*
			Posterior	78.8	
			Left	77.6	0.51
			Right	78.7	
			Base	79.2	<0.001*
			Mid	80.4	
			Apex	74.6	
	PPV (%)	Whole Prostate		67.4	-
		Transition Zone		67.0	0.71
		Peripheral Zone		66.4	
		TZ	Anterior	66.2	0.47
			Posterior	68.5	
			Left	67.0	0.98
			Right	67.1	
			Base	68.6	0.86
			Mid	66.4	
			Apex	67.0	
		PZ	Anterior	72.7	<0.001*
			Posterior	65.0	
			Left	65.8	0.55
			Right	66.9	
			Base	63.5	0.43
			Mid	66.6	
			Apex	67.0	